Hindawi Publishing Corporation
Journal of Spectroscopy
Volume 2015, Article ID 184140, 13 pages
http://dx.doi.org/10.1155/2015/184140

Research Article

Effect of the Unsaturation of the Hydrocarbon Chain of Fatty-Amides on the CO_2 Corrosion of Carbon Steel Using EIS and Real-Time Corrosion Measurement

J. Porcayo-Calderon,[1,2] I. Regla,[2,3] E. Vazquez-Velez,[2] L. M. Martinez de la Escalera,[4] J. Canto,[4] and M. Casales-Diaz[2]

[1]*CIICAp, Universidad Autonoma del Estado de Morelos, Avenida Universidad 1001, 62209 Cuernavaca, MOR, Mexico*
[2]*Instituto de Ciencias Fisicas, Universidad Nacional Autonoma de Mexico, Avenida Universidad s/n, 62210 Cuernavaca, MOR, Mexico*
[3]*Facultad de Estudios Superiores Zaragoza, Universidad Nacional Autonoma de Mexico, Avenida Guelatao 66, 09230 Mexico City, DF, Mexico*
[4]*Corrosión y Protección (CyP), Buffon 46, 11590 Mexico City, DF, Mexico*

Correspondence should be addressed to J. Porcayo-Calderon; jporcayoc@gmail.com

Received 2 December 2014; Accepted 17 February 2015

Academic Editor: Stephen Cooke

Fatty-amide derivatives were evaluated to study the effect of the double bonds into the hydrocarbon chain (C18) on the corrosion behavior of carbon steel. Electrochemical impedance spectroscopy (EIS) and real-time corrosion measurements were used to evaluate the inhibition mechanism of the fatty-amides on carbon steel in CO_2-saturated (3% NaCl + 10% diesel) emulsion at 50°C. EIS results demonstrated that the unsaturation present into the hydrocarbon chain contributes to the efficiency of fatty-amides, because they can be adsorbed on the metal surface by a flat-adsorption process reducing the presence of active sites and blocking the corrosion process and preventing the diffusion of corrosive species, such as H_2O, H^+, Cl^-, and HCO_3^-. Real-time corrosion measurements also indicated that the effectiveness of the inhibitors is dependent on the unsaturation into the hydrocarbon chain, being also a good technique to determine the stability of the adsorption process of the inhibitors.

1. Introduction

The use of corrosion inhibitors is the most practical and economical method for corrosion protection and prevention of unexpected metal dissolution in aggressive media. The presence of such inhibitor retards the corrosion process and keeps the corrosion rate at a minimum, thus preventing economic losses due to metallic corrosion. One of the most aggressive environments found in the petroleum industry is the fluids with high concentrations of chlorides and carbon dioxide, which leads to called CO_2 corrosion or sweet corrosion [1, 2].

It has been known that the organic molecules can be adsorbed at the metal-electrolyte interface, thereby inhibiting corrosion onto metal surface [3]. Effectiveness of organic inhibitors depends upon its adsorption rate and surface coverage. Inhibitors are adsorbed by replacing the water molecules onto the metal surface. Adsorption is determined by the molecular structure, surface charge of the metal, and type of electrolyte. Many factors are involved during this action, the electrostatic interactions between the inhibitor molecules and the metal, the electron densities of the different functional groups, polarizability, and electronegativity. Nitrogen-based organic surfactants, such as imidazolines, amides, amide-amines, and amines and their salts, have been used successfully as inhibitors in oil field applications and several researches are focusing their efforts on the development of environmental friendly inhibitors [4–7].

In the literature, studies about the stability (hydrolysis) of imidazolines and imidazoline-based products have been performed. Butler et al. [8] reported the conversion of fatty unsaturated imidazolines to amides precursors at room temperature conditions over 2 to 9 days. However, Bondareva et al. [9] studied the kinetics of hydrolysis of

imidazolines (pH 2.0–12.5, T = 70–90°C), and their results showed that the hydrolysis occurred at basic pH but at acid pH (<6) it was not observed. Presumably, the stability of the imidazoline can be related to protonation at the tertiary N atom in the imidazoline ring; this positive charge on the N atom prevents hydrolysis. It has been reported that the hydrochloride salts of imidazoline are more resistant to hydrolysis than the free imidazolines, and the activity of the imidazoline-based and amide-based products is similar; however, some authors have found that amide precursors have better efficiency than the imidazoline precursors [10]. Martin and Valone [10] have shown via 13C NMR, FT-IR, and UV spectroscopy that the imidazolines are converted into their amide precursor after its reaction with acid, and there is no significant difference in the performance of both inhibitors formulated. Jovancicevic [7] determined the effect of the hydrophobic group of palmitic amide/imidazoline on the corrosion rate. They reported that the contribution of the amide group is more significant than that of the imidazoline group in the corrosion inhibition. Similar results were obtained with the hydrolyzed stearic imidazoline and stearic amide, suggesting a substantial hydrolysis of imidazoline in <45 min under CO_2-saturated brine conditions (pH = 6.3) (T = 66°C). Similar corrosion rates were obtained after 45 min and 60 min hydrolysis. Therefore, if the performance of inhibitors formulated with an imidazoline or its amide precursor is similar, the use of amide inhibitor reduces the cost of inhibitor.

On the other hand, the study of the structure-performance relationship of imidazolines and corresponding amides has been an interesting subject as well as the role of the hydrocarbon chain relative to the imidazoline head group and the pendant amine group in film formation [2–11]. Jovancicevic reported that the corrosion inhibition is enhanced with the increasing number of carbon atoms in the alkyl chain (C12 versus C18) of imidazolines. The effect of the hydrophilic head group (imidazoline, amide, and amine) was studied for a specific chain. The results showed that the palmitic imidazoline was less effective than the palmitic amine and the palmitic amide. Ebenso et al. reported that the efficiency of inhibition may be increased by increasing the number of substituents of the functional groups and the nature of the electron donor [12]. Few studies have been reported about the effect of the double bond of the hydrocarbon chain, of either fatty-amides or imidazolines, on the inhibition efficiency [3]. Yoo et al. evaluated the effect of the double bond of the hydrophobic chain of imidazolines on the corrosion performance. Therefore, the aim of this study is to investigate the effect of the double bonds in the hydrocarbon chain of fatty-amides in the electrochemical behavior of the carbon steel in CO_2-saturated (3% NaCl + 10% diesel) emulsion at 50°C. For this, a series of amides were synthesized from pure fatty acids C18 for their study as inhibitors.

2. Experimental Procedure

2.1. Material. Material tested was a 1018 carbon steel cylinder measuring 25 mm in length and 5.0 mm diameter. Before testing, the electrode was polished to 600 grit SiC emery paper and then cleaned with alcohol, acetone, and distilled water. Specimens with this surface condition were employed as the working electrode (WE) in the electrochemical tests.

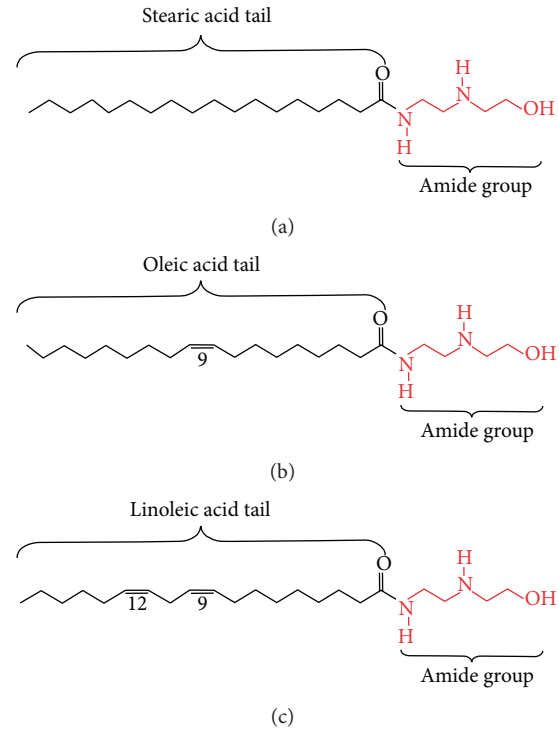

Figure 1: Molecular structure of the fatty-amides evaluated: (a) stearic amide (18 : 0), (b) oleic amide (18 : 1 n-9), and (c) linoleic amide (18 : 2 n-6).

2.2. Test Solution. Three types of inhibitors were used in this study (Figure 1). The inhibitors were dissolved in water at pH 4.0. The testing solution consisted of 90 : 10 (v/v) mixture of 3% NaCl solution and diesel, respectively. The solution was saturated with CO_2 for 2 h before testing and kept under a CO_2 atmosphere during testing. For the experiments, the cell temperature was kept constant at 50°C. The solutions were stirred continuously. The working electrode was kept in the electrolyte for 1 h before any inhibitor containing the solution was introduced. The concentration of the inhibitor used in this work was 25 ppm.

2.3. Electrochemical Measurements. For each electrochemical test a volume of 600 mL of fresh solution was used. In this study the conventional electrochemical techniques employed were open-circuit potential (OCP), linear polarization resistance (LPR), and electrochemical impedance spectroscopy (EIS) measurements. Measurements were obtained by using a conventional three-electrode glass cell. A saturated calomel electrode (SCE, 0.242 V versus SHE) was used as the reference electrode with a Luggin capillary bridge, and a high density and high surface area graphite rod was used as the counter electrode. The tip of the Luggin capillary is made very close to the surface of the working electrode to minimize IR drop.

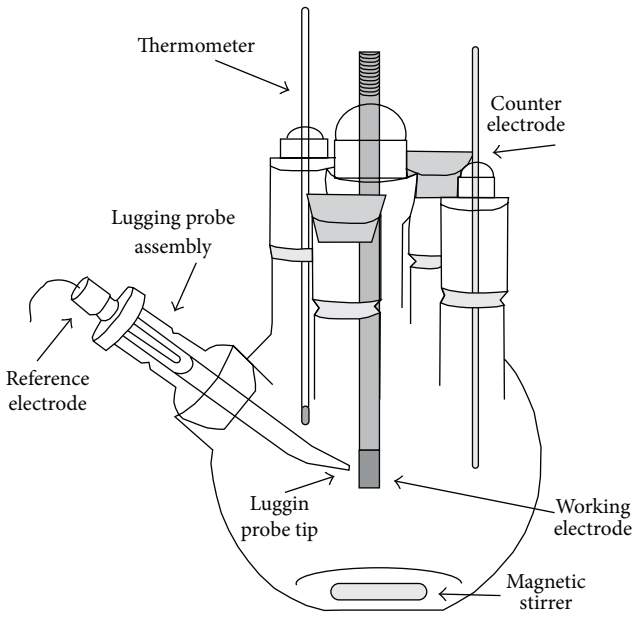

Figure 2: Experimental set-up for electrochemical measurements.

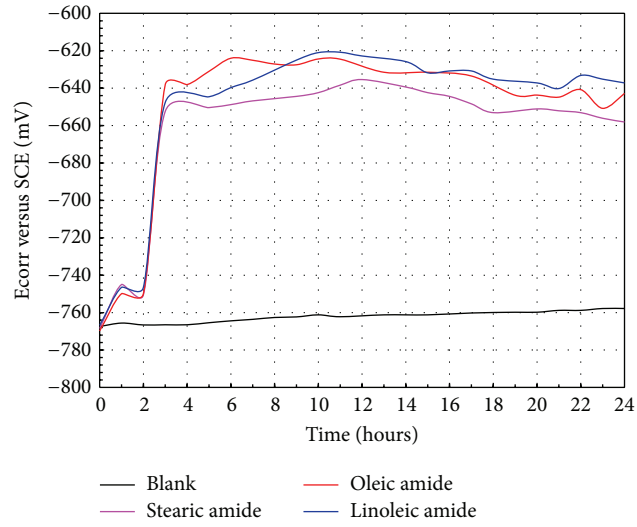

Figure 3: Change of the E_{corr} values as function of testing time for 1018 carbon steel in CO_2-saturated (3% NaCl + 10% diesel) emulsion with and without fatty-amides at 50°C.

The electrochemical cell used was that described by standard ASTM G5 and shown in Figure 2. For LPR measurements, a sweep from −20 to +20 mV versus open-circuit potential at a sweep rate of 1.0 mVs^{-1} was used and the polarization resistance (R_p) was measured from the slope of potential-current curve in the vicinity of corrosion potential (E_{corr}). Measuring the variation with time the open-circuit potential (OCP) of the working electrode was also performed. LPR and OCP measurements were conducted every 60 min during 24 hours. Impedance measurements were carried out using AC signals of amplitude 10 mV peak to peak at the open-circuit potential in the frequency range 100 kHz to 1.0 mHz. LPR, OCP, and EIS experiments were carried out using Interface 1000 Gamry Potentiostat/Galvanostat/ZRA analyzer.

2.4. Real-Time Corrosion Measurement. Continuous electrochemical corrosion was also monitored using a three-electrode (finger) probe arrangement with three identical 1018 carbon steel electrodes. The multitechnique electrochemical monitoring instrumentation (SmartCET) employs a combination of electrochemical noise (EN), linear polarization resistance (LPR), and harmonic distortion analysis (HDA) to provide output of a general corrosion rate and localized corrosion behavior (pitting factor). The measurement cycle takes place over a period of 430 seconds, as follows: current and potential noise measurement, second-by-second for 300 seconds, LPR/HDA measurement for 100 seconds, and solution resistance (R_s) measurement for 30 seconds. Details of this technique for monitoring real-time are described elsewhere [13, 14]. Interpretation of pitting factor (PF) value is in accord with the following.

(i) PF < 0.01 represents general corrosion.
(ii) PF in the range 0.01 to 0.1 represents an intermediate zone but dominates general corrosion.
(iii) PF > 0.1 represents localized corrosion.

3. Results and Discussion

3.1. OCP versus Time Measurements. In the present study, the variation of the OCP of carbon steel was followed as a function of time in CO_2-saturated (3% NaCl + 10% diesel) emulsion with and without fatty-amides at 50°C. Results obtained are depicted in Figure 3.

In fatty-amides free emulsion, the OCP changed slowly towards more positive values, indicating the growth of an oxide film on the carbon steel surface which provides some protection against corrosion. In all cases, with the addition of fatty-amides, a displacement of +30 mV was observed in the first hour; after that, an apparent lag phase is observed for one hour, and from this point an abrupt increase of about +100 mV in the E_{corr} values is observed. Subsequently, an oscillation of ±10 mV in E_{corr} is observed for the rest of the corrosion test. Usually a rise of E_{corr} in the positive direction indicates the formation of a passive film, and a steady E_{corr} indicates that the film remains intact and protective, and a drop of E_{corr} in the negative direction indicates breaks in the film, dissolution of the film, or no film formation [15]. On the other hand, according to Riggs Jr. [16] and others [17, 18], the classification of a compound as an anodic or cathodic type inhibitor is feasible when the OCP displacement is at least 85 mV in relation to that one measured for the blank solution; if displacement in E is <85 mV, the inhibitor can be seen as mixed type. From OCP measurements it is possible to say that the tested fatty-amides decrease the anodic dissolution of iron, causing appreciable changes on E_{corr} values. This is owing to the formation of a protective film onto carbon steel surface and acting as a protective barrier. as Although the magnitude of changes in the E_{corr} values is similar, the degree of unsaturation of the oily tail of the fatty-amide seems that influences its E_{corr} values, being linoleic amide > oleic amide > stearic amide.

3.2. LPR Measurements. In order to determine the polarization resistance, the working electrode was polarized ±20 mV around the open-circuit potential at a scan rate of 1.0 mVs^{-1}. Measurements were conducted in CO_2-saturated (3% NaCl + 10% diesel) emulsion without and with the three tested inhibitor at 50°C. Since the voltage-current response of the corroding electrode tends to be linear over a small range of potentials at either side of the free corrosion potential, then the slope of the potential/current sweep is measured to provide the polarization resistance, which is inversely proportional to the corrosion current density. Polarization resistance results obtained are depicted in Figure 4. On the other hand, the inhibition efficiencies (Figure 5) of the tested fatty-amides were calculated from (R_p) values obtained from the LPR data based on the following relation:

$$E\,(\%) = \frac{R_{p,i} - R_{p,b}}{R_{p,i}} * 100, \quad (1)$$

where $R_{p,b}$ is the linear polarization resistance without inhibitor and $R_{p,i}$ is the linear polarization resistance with inhibitor.

In fatty-amides free emulsion, corrosion resistance of carbon steel slowly decreases as time evolved, indicating that the growth of the oxide film on the steel surface does not act as protective barrier and is permeable to the diffusion of aggressive ions. With the addition of fatty-amides, similar behavior to that of the OCP measurements was obtained, that is, an abrupt increase in R_p values in the first hour, after that, a slight decrease for one hour, and from this point a constant increase as time evolved. In the first two hours the observed behavior can be due to the rapid formation of a protective inhibitor film onto metal surface. However, when the adsorbed inhibitor molecules exceed certain number, the molecules can be so close that electrostatic repulsion forces can occur leading to the desorption of the inhibitor molecules. This electrostatic repulsion forces could cause the appearance of unprotected sites on the metal, which provokes their corrosion. Subsequently it is possible that unprotected sites were covered by the ordered adsorption of inhibitor molecules. Similar observations have been made by other authors [17], since they indicate that when more inhibitor molecules adsorb, the adsorption density of surfactant becomes so high that interaction between tails of the surfactant may occur leaving the surface and causing the decrease of the effective area covered by the inhibitor molecule to some extent. Some authors suggest [19] that the decrease in the inhibition efficiency can be attributed to the orientation change of inhibitor molecules onto the metallic surface and some others to the induction of the corrosion process as a result of permeation of the electrolyte through the inhibitor protection layer [20]. From R_p measurements, apparently again the degree of unsaturation of the oily tail of the fatty-amide influenced the corrosion rate of carbon steel in the following order: linoleic amide > oleic amide > stearic amide.

The increase in the R_p value suggests that the inhibition efficiency increases with the degree of unsaturation of the oily tail of the fatty-amide. From Figure 5, it can be noted that

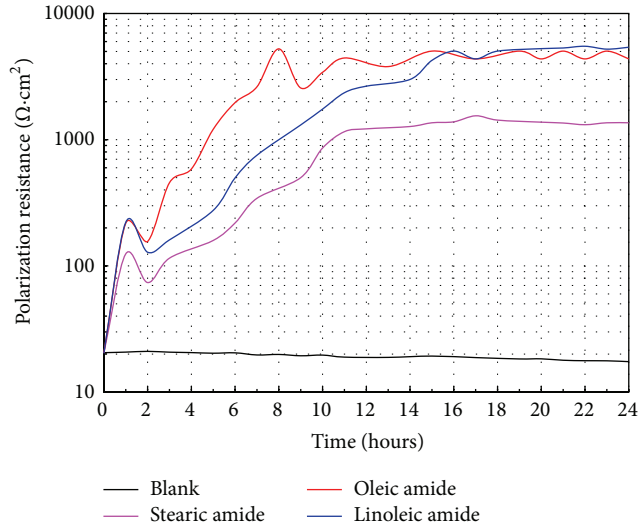

Figure 4: Change of R_p values function of testing time for 1018 carbon steel in CO_2-saturated (3% NaCl + 10% diesel) emulsion with and without fatty-amides at 50°C.

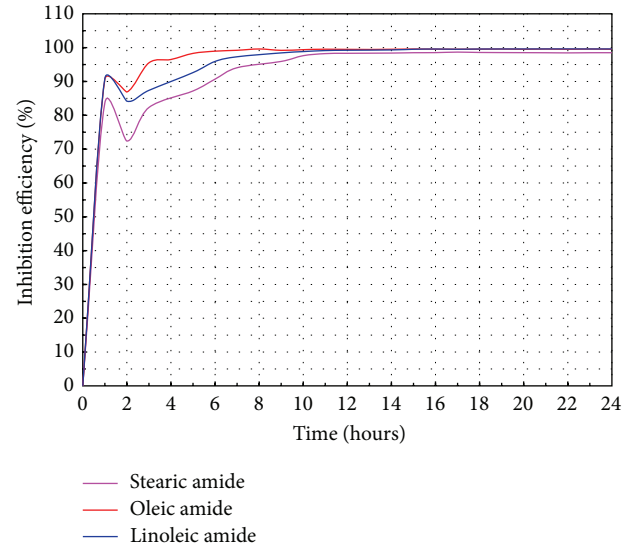

Figure 5: Variations of inhibition efficiency as determined by LPR measurements.

after reaching the steady state, the protection efficiency of the fatty-amides was over 98%, being 99.62% for linoleic amide, 99.53% for oleic amide, and 98.50% for stearic amide. These findings reveal that the fatty-amide has a high affinity for the metallic surface, since its adsorption onto the electrode surface was relatively fast and the formation of a protective film with excellent barrier properties is evident.

3.3. Impedance Measurements. Electrochemical impedance spectroscopy measurements were performed in order to gain a better understanding of the corrosion and corrosion inhibition of carbon steel in CO_2-saturated (3% NaCl + 10% diesel) emulsion at 50°C. Bode plots for carbon steel

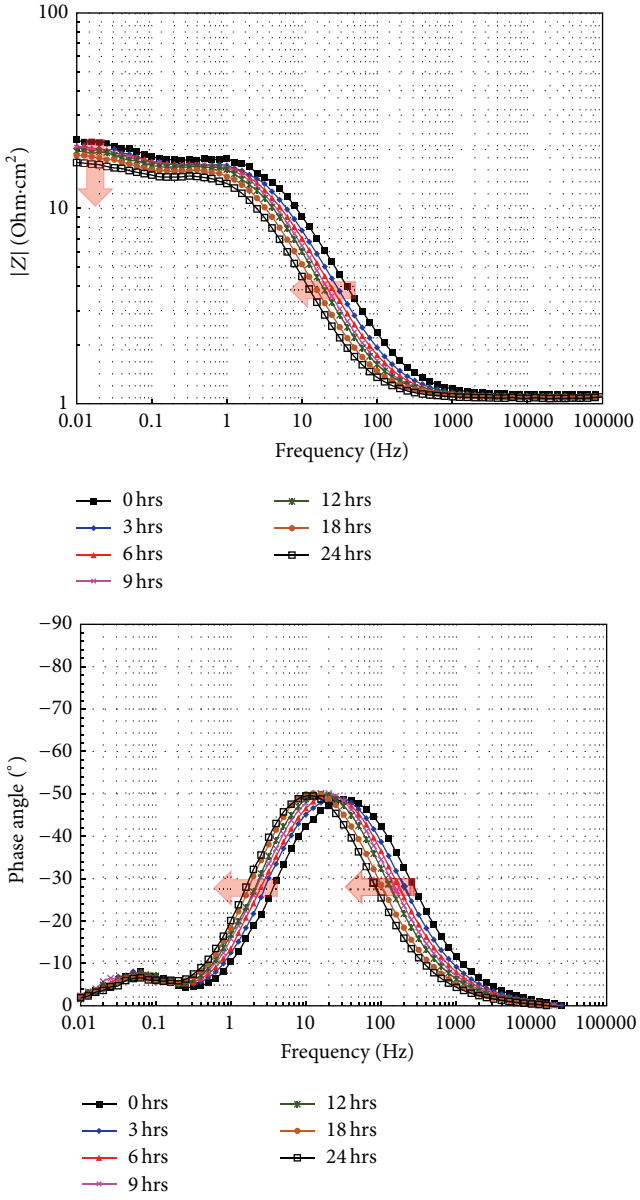

FIGURE 6: Nyquist and Bode plots for 1018 carbon steel in CO_2-saturated (3% NaCl + 10% diesel) emulsion without inhibitors at 50°C.

exposed to CO_2-saturated (3% NaCl + 10% diesel) emulsion at 50°C are shown in Figure 6. In general, three frequency regions referring to as the high, intermediate, and low frequency values are observed from Bode diagrams [21]. In the high frequency region the $\log|Z|$ values tend to a constant where the phase angle approaches zero. The constant value observed corresponds to the solution resistance (R_S). In the intermediate frequency region, there is a linear relationship between $\log|Z|$ and $\log f$, where the slope value is lower than −1, and phase angle value less than 90°, indicating that the protective oxide layer has no capacitive nature and that the corrosion process can be under mixed control (diffusion and charge transfer). A maximum in the phase angle which is slightly shifting to lower frequencies as time elapses (30 to 10 Hz) is observed; this displacement is coupled with both a slight increase of the phase angle and a steady decrease in the slope of the $\log|Z|$-$\log f$ relation. Because this is the characteristic response of capacitive behavior of the electrode surface and describes the dielectric properties of the electronically conducting surface film, this shift can be associated with a detachment, or thinning of the protective films [22, 23]. In the low frequency region as time elapses, the $\log|Z|$ values show a tendency to decrease but the evolution of a new capacitive loop also is observed. In this region are detected the electron charge transfer processes, the mass transfer processes, or other relaxation processes taking place into the film-electrolyte interface or within the pores of the surface film. This is evidence of the nonprotective nature of the corrosion products. The main formed film during CO_2 corrosion of carbon steels is iron carbonate, $FeCO_3$. Thus, it seems that $FeCO_3$ scale is not fully formed on the steel surface, and therefore the corrosion rate shows slight increases. The formation of new capacitive loop may indicate the presence of a surface process that may be affecting the corrosion process. This confirms that the corrosion process can be influenced by both charge transfers as diffusion. Nyquist diagrams (not shown) showed that, in the high and intermediate frequency values, the data describes a depressed, capacitive-like semicircle, with its center at the real axis, indicating that the corrosion process is under charge transfer control from the metal surface to the environment through the double electrochemical layer. Also, as time elapses its diameter decreases, increasing the corrosion rate. However, at lower frequency values, the presence of a new capacitive-like semicircle was evident. Its lower capacitance could be attributed to adsorption phenomena of intermediate species as FeOH due to the hydrolysis of Fe during the metal dissolution process [24] or to the presence of the water-soluble fractions (WSFs) of the oil phase, which can be adsorbed on the steel surface thereby reducing the corrosion rate, besides affecting the mass transfer processes [23].

Figure 7 shows the Bode plots for carbon steel exposed in the CO_2-saturated (3% NaCl + 10% diesel) emulsion with 25 ppm of stearic amide as inhibitor at 50°C. In the high frequency range, as time elapses, it is observed that the plateau region begins to form at higher frequencies than 10,000 Hz. At the same time, the phase angle-frequency relationship shows the evolution of a new loop and its value increases over time. The formation and evolution of the new loop are owing to the self-assembling of inhibitor molecules onto the carbon steel surface. Because the inhibitor film formed is a layer of oily nature its formation is detected in the high frequency region. The protective ability of the inhibitor molecules depends on its solubility and rate of transport toward the surface of the carbon steel. However in the case of oil-soluble inhibitors the presence of the WSFs can affect the growth rate of the protective film and thus reduce its efficiency. It is observed that the phase angle maximum value increases slowly as time elapses and the loop appears around 1,000–2,000 Hz. The maximum value of the phase angle was 58°. This suggests both a slow growth and low capacitance of the protective film. In the intermediate frequency region,

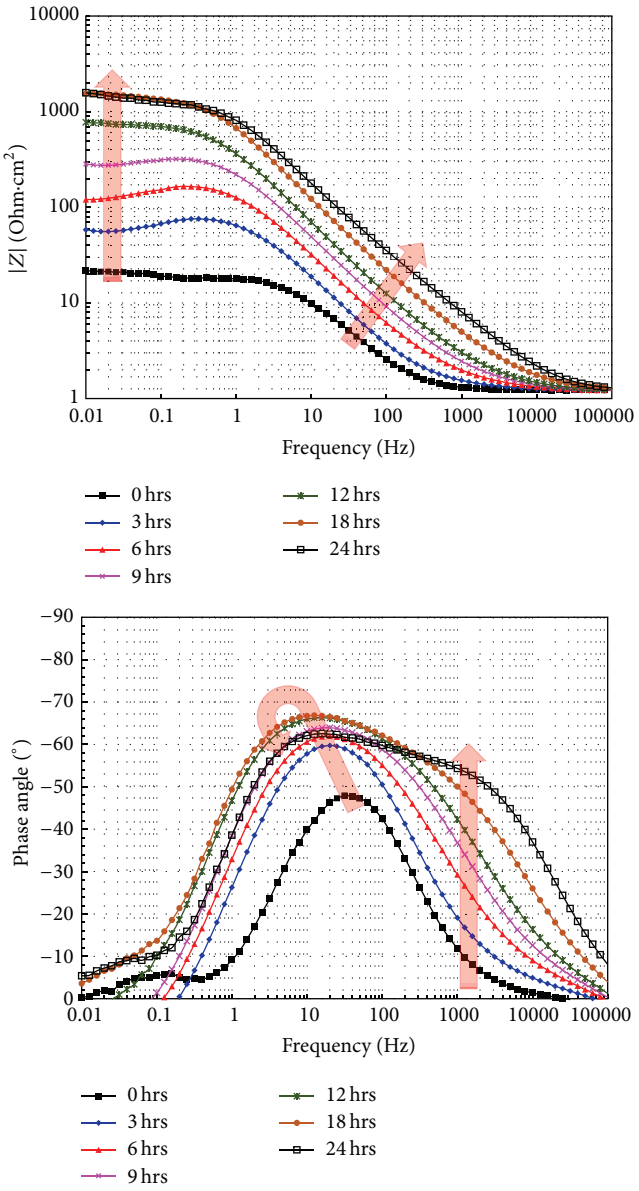

Figure 7: Nyquist and Bode plots for 1018 carbon steel in CO_2-saturated (3% NaCl + 10% diesel) emulsion with 25 ppm of stearic amide at 50°C.

there is a linear relationship between $\log|Z|$ and $\log f$, and only one slope is observed. The values of slopes are higher than those observed in the uninhibited solution, indicating that the layers formed onto steel surface are more protective than those developed in the uninhibited solution. Phase angle-frequency relationship also shows the presence of one loop and its maximum value increases from 48° to 68° until 18 hours and then slightly decreases to 63°. On the other hand, a shift to lower frequencies of the intermediate loop from 35 Hz to around 15 Hz is observed. It is interesting to note that in inhibited solution the maximum value of phase angle was 50° (Figure 6). The characteristics of evolution of this loop can be associated on the basis of a flat-adsorption process of the inhibitor, where the adsorbed layer is assumed to cover the entire surface quickly and, at the same time, blocks access to the active site of corrosion on the surface, reducing the aggressiveness of attack at these sites [25]. This may explain the increase in the maximum value of phase angle. In the low frequency region, the impedance module ($|Z|$) increased to three orders of magnitude compared to those of uninhibited solution. This indicates the protective nature of the inhibitor film due to the packing efficiency of the molecules of the inhibitor onto metal surface.

Figures 8 and 9 show the Bode plots for carbon steel exposed in the CO_2-saturated (3% NaCl + 10% diesel) emulsion at 50°C for oleic amide and linoleic amide, respectively. Characteristics of the impedance spectra are similar to those observed with the addition of stearic amide inhibitor; that is, at the high frequency range, the plateau region begins to form at higher frequencies than 10,000 Hz, and the evolution of a new loop is observed, with similar values of phase angle. In the intermediate frequency region, the phase angle-frequency relationship also shows the presence of one loop and its value increases and then slightly decreases. Also, a shift to lower frequencies of the intermediate loop is observed. The low value of phase angle of this loop suggests that there is some permeability. In the low frequency region, also the impedance module ($|Z|$) increased to three orders of magnitude compared to those of uninhibited solution, indicating the protective nature of the inhibitor film. Based on the similar behavior of the three fatty-amides, it can be assumed that the protective mechanism is the same. At this point, it can be assumed that fatty-amides are adsorbed rapidly by a process of flat adsorption onto the metal surface increasing its corrosion resistance (phase angle increased in the intermediate frequency region), and the oily tail forms a hydrophobic barrier repelling to the aggressive ions from the bulk solution.

3.4. Analysis of Impedance Data. Interpretation of the electrochemical behavior of a system from EIS spectra requires an appropriate physical model of the electrochemical reactions into the electrode surface. In this sense, the equivalent circuits are used to model the electrochemical behavior and calculate the parameters of interest, such as electrolyte resistance (R_s), charge transfer resistance (R_{ct}), and double layer capacitance (C_{dl}). However, when a nonideal frequency response is present, it is accepted to employ distributed circuit elements in an equivalent circuit. The most widely used is the constant phase element (CPE). CPE is used in a model in place of a capacitor to compensate the inhomogeneity in the system which takes into account the irregularities of the surface such as roughness or because properties such as double layer capacitance, charge transfer rate are nonuniformly distributed. CPE is an element whose impedance value is a function of the frequency and whose phase is independent of the frequency and its impedance is defined as

$$Z_{\mathrm{CPE}} = \frac{1}{Y_0}(i\omega)^{-n}, \tag{2}$$

where Y_0 is a proportional factor that indicates the combination of properties related to both the surfaces and

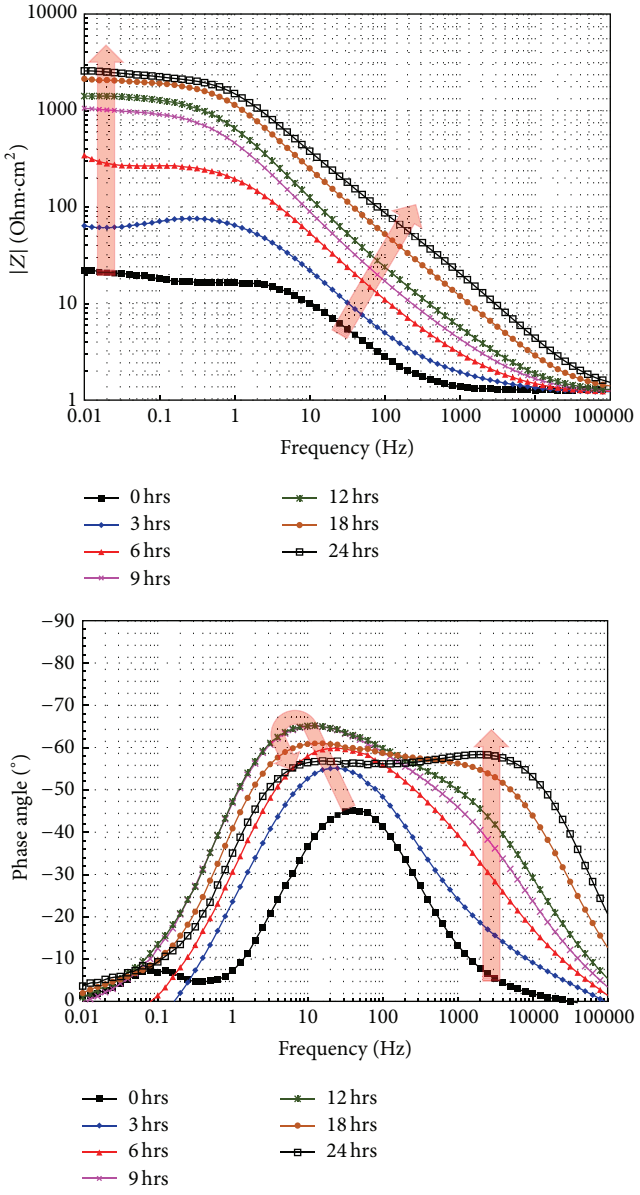

Figure 8: Nyquist and Bode plots for 1018 carbon steel in CO_2-saturated (3% NaCl + 10% diesel) emulsion with 25 ppm of oleic amide at 50°C.

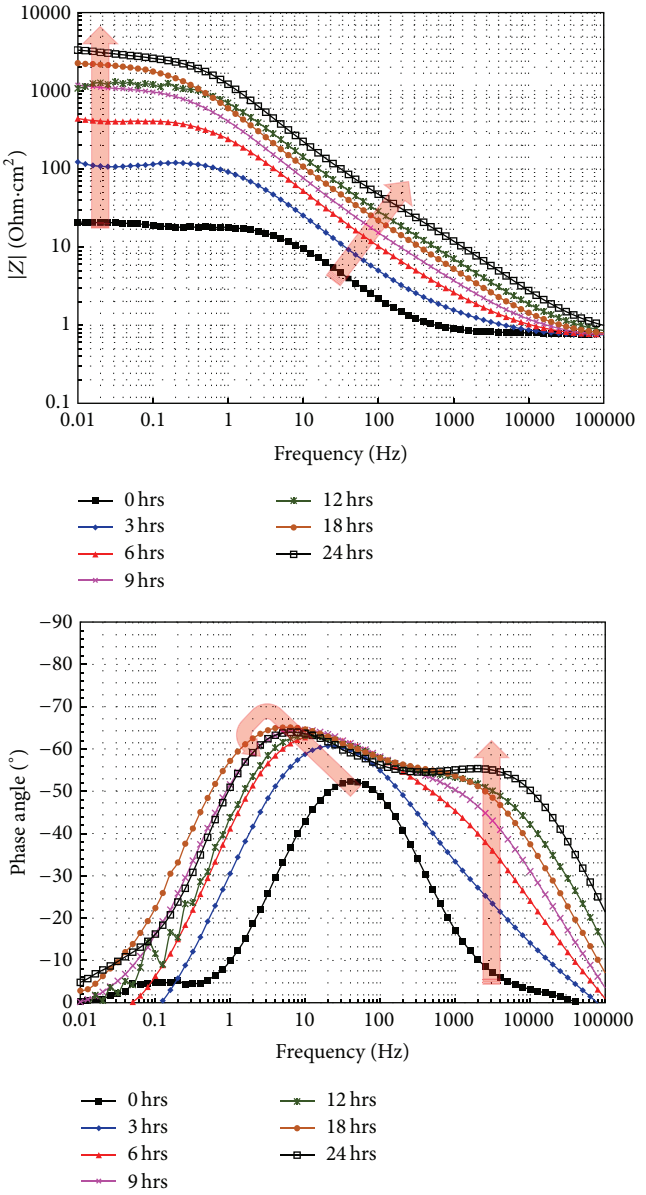

Figure 9: Nyquist and Bode plots for 1018 carbon steel in CO_2-saturated (3% NaCl + 10% diesel) emulsion with 25 ppm of linoleic amide at 50°C.

electroactive species independent of frequency; i is imaginary number ($\sqrt{-1}$); ω is the angular frequency and equal to $2\pi f$, where f is the frequency; and n has the meaning of a phase shift and is related to a slope of the log $|Z|$ versus log f plots and usually is in the range 0.5 and 1. When the value of n is equal to 1, the CPE describes an ideal capacitor with Y_0 equal to the capacitance. For $0.5 < n < 1$ the CPE describes a distribution of dielectric relaxation times in frequency space, and when n is equal to 0.5 the CPE represents Warburg impedance with diffusional character. In these situations the semicircle in the Z_{re}-Z_{im} spectra is more and more depressed and the depression degree depends on the phase of the CPE [26].

According to results for metal electrodes corroded without the presence of inhibitor there were two time constants (Figure 6), where the first one was related to the corrosion process at the metal/corrosion products/electrolyte interphase and the second one was attributed to adsorption phenomena of intermediate species or to the presence of the WSFs which affect the mass transfer processes. Therefore the equivalent circuit used is shown in Figure 10, where a finite length Warburg (FLW) element was included:

$$Z_W = \frac{R_W * \tanh\left(\left[\sqrt{-1} * T * \omega\right]^P\right)}{\left(\sqrt{-1} * T * \omega\right)^P}. \quad (3)$$

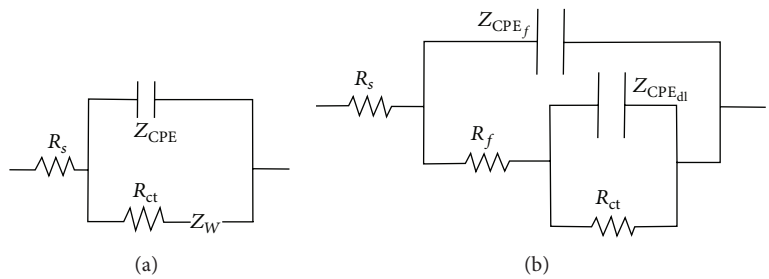

FIGURE 10: Equivalent circuits; (a) metal electrodes corroded without inhibitor; (b) metal electrodes corroded in presence of inhibitor.

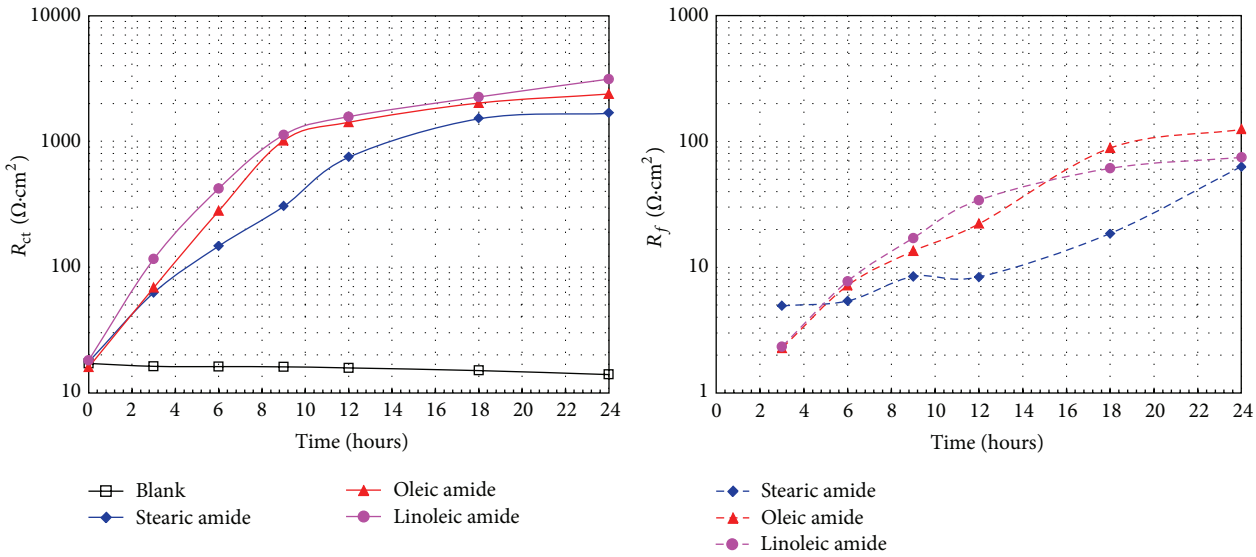

FIGURE 11: R_{ct} and R_f variation against time for carbon steel with and without fatty-amides.

FLW is the solution of the one-dimensional diffusion equation of a particle, where $T = L^2/D$ (L is the effective diffusion thickness, and D is the effective diffusion coefficient of the particle), $P = 0.5$. This version of the Warburg element terminates in a finite resistance where at very low frequencies, Z_{re} approaches R_W and Z_{im} goes to zero.

On the other hand, for metal electrodes corroded in presence of inhibitor, from phase angle versus frequency plot, two separate peaks can be clearly seen indicating the existence of two time constants (Figures 7 to 9). High frequency time constant indicates the presence of the fatty tail of the inhibitor film in contact with the electrolyte, and the intermediate and low frequency one is related to corrosion process at the unprotected sites of the metal surface. In this case, the time constants can be modelled by the equivalent circuit shown in Figure 10(b). Because some studies [27] indicate that between the hydrophobic tails there is a gap of about 0.4–0.6 nm, that is why that the equivalent electrical circuit represent a porous inhibitor film formed onto the metal surface, in which Z_{CPE_f} is related to the nonideal capacitance of the inhibitor film, R_f to the inhibitor film resistance, which reflects the protective properties of the inhibitor film, and $Z_{CPE_{dl}}$ to the nonideal capacitance of the double layer of the electrolyte/corrosion products/metal interphase. In this case, $R_f < R_{ct}$; hence $Y_0 = Y_f + Y_{dl} \sim Y_{dl}$ [23, 28, 29]. The evolution of the fitting parameters obtained using the electrical circuits shown in Figure 10 is presented in Figures 11 to 13.

Figure 11 shows the variation of R_{ct} and R_f with and without fatty-amides. From R_{ct} plot it can be seen that carbon steel showed the lowest corrosion resistance, and its R_{ct} values tend to decrease as time elapses. This is because the corrosion product layer was not protective; it is known that, at 50°C, these scales are porous and nonhomogeneous, allowing the access of the corroding solution to the base material [28]. However, in the presence of the inhibitors, regardless of the type of fatty-amide added, it can be seen that the corrosion resistance of the carbon steel is increased until two orders of magnitude. R_{ct} values tend to increase continuously without reaching the steady state. The observed increase in the R_{ct} values indicates an efficiency protection around of the 99.0%. R_{ct} values depended on the degree of unsaturation of the fatty-amide, being linoleic amide > oleic amide > stearic amide. On the other hand, the R_f values observed are lower with respect to those of R_{ct}. This is consistent because the oily tail is the only component of the inhibitor-adsorbed which is in contact with the electrolyte, and this it is an oily film of a few angstroms thick. This is the reason why its presence will always be detected in the high frequency region.

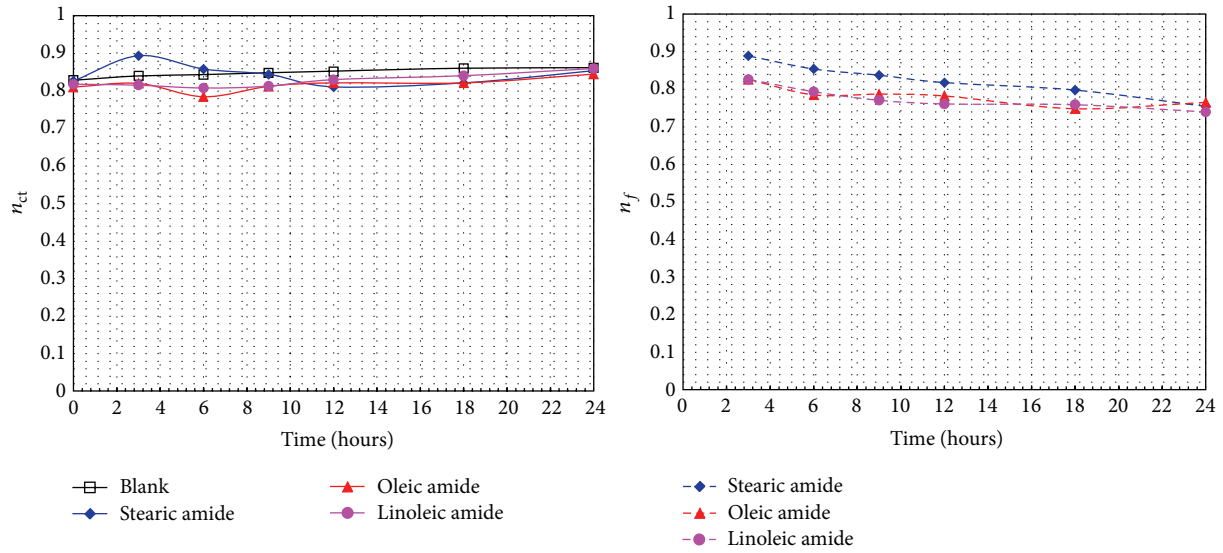

FIGURE 12: n_{ct} and n_f variation against time for carbon steel with and without fatty-amides.

Again, the R_f values depended on the degree of unsaturation of the fatty-amide, being linoleic amide > oleic amide > stearic amide. That is, the presence of unsaturations favors the formation of more dense and compact inhibitor films.

Figure 12 shows the n_{ct} and n_f variation with and without fatty-amides. When the value of n is equal to 1 the CPE describes an ideal capacitor, and when n ranges from 0.5 to 1.0 the CPE describes a distribution of dielectric relaxation times in frequency space, and when n is equal to 0.5 the CPE represents Warburg impedance with diffusional character. On this basis, it can be seen that in the absence of fatty-amides the n_{ct} values are greater than 0.8 and show a tendency to increase. Therefore the corrosion process is controlled by charge transfer ($n_{ct} > 0.8$), and it is possible to say that the intermediate species and the WSFs adsorbed do not affect the corrosion process because the diffusion resistance (R_W) determinate was around 3 ohms. However, in the presence of fatty-amides the n_{ct} values were similar but slight lower, indicating that the corrosion process in unprotected sites was also controlled by charge transfer. On the other hand, the values of n_f were lower than n_{ct} values and showed a tendency to decrease. The n_f values of the unsaturated fatty-amides were lower than those of the saturated fatty-amide.

The proportional factor, Y_0, is independent of the frequency and it represents a combination of properties related to both the surfaces and the electroactive species, and when the value of n is equal to 1, it is the capacitance. CPE is related to the capacitance (C_i) according to the following equation [30]:

$$C_i = \left(Y_{0i} R_i^{(1-n_i)}\right)^{1/n_i}. \quad (4)$$

On the basis of this equation, the double layer capacitance (C_{dl}) and the capacitance of the film (C_f) involved in the two CPEs (CPE_{dl} and CPE_f) can be calculated.

Figure 13 shows plots of the capacitance (CPE_{dl} and CPE_f) versus time with and without fatty-amides. Generally in corrosion tests without inhibitor the diameter of the high frequency semicircle is treated as the charge transfer resistance R_{ct}, and in corrosion tests with inhibitor the high frequency capacitive loop is related to the barrier and properties of the inhibitor layer [31]. From Figure 13 it can be seen that the capacitance (C_{dl}) of the carbon steel without the presence of fatty-amides shows a steady increase in their values as time elapsed. However, in the presence of fatty-amides, the capacitance values are lower, and their values tend to a constant value. On the other hand, the capacitance values of the inhibitor film (C_f) are lower than those of carbon steel without addition of fatty-amides, and their values tend to decrease as time passes. It is clear that the presence of the fatty-amides has a marked effect on the values of the capacitance. Capacitance values (C_{dl} and C_f) in the presence of fatty-amides have almost the same values and all shown the same trend. It is known that a decrease in the capacitance can happen if the inhibitor molecules (low dielectric constant) replace the adsorbed water molecules (high dielectric constant) on the carbon steel surface [32]. This behavior supports the flat-adsorption process of the fatty-amides, where the adsorbed layer covers the surface quickly, blocking the access to the active site and improving the corrosion resistance of the carbon steel [25]. Since the capacitance is inversely proportional to the thickness of the double layer, a decreasing in the capacitance values could be attributed to the adsorption of the fatty-amide onto the metal surface. When the fatty-amide is added into the electrolyte the active sites are covered forming a smooth surface, and consequently the capacitance decreases. In general, the surface area of a rough and porous electrode is large and the capacitance is high compared to that on a smooth surface. It is possible that the fatty-amide can be adsorbed on the Fe surface through the amide group and the oily chain both approximately perpendicular to the surface and blocking also active sites by a flat-adsorption process. Therefore, with time, fatty-amide molecules adsorb

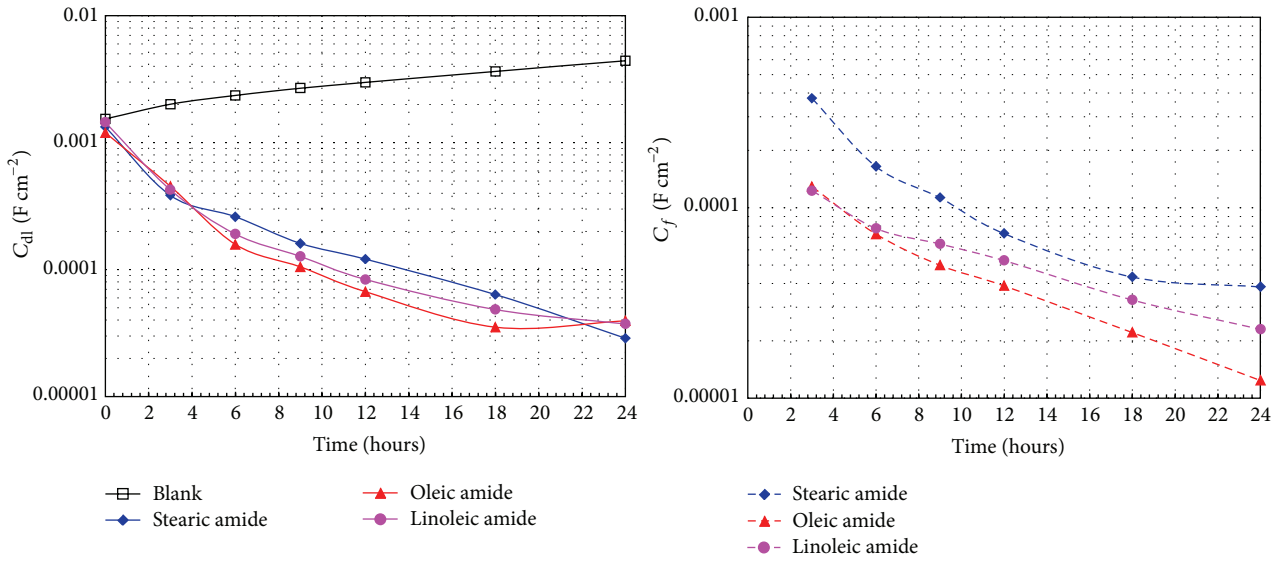

FIGURE 13: C_{dl} and C_f variation against time for carbon steel with and without fatty-amides.

on the metal surface and the protective film grows until it covers all possible corroding sites by forming a thin film on the metal surface, hence reducing the capacitance values. The capacitance values (C_{dl} and C_f) of the unsaturated fatty-amides were lower than those of the saturated fatty-amide.

From these results, it is possible to establish that the unsaturation present in the oily tail contributes to the efficiency of fatty-amides, because they can be adsorbed on the metal surface by a flat-adsorption process reducing the presence of active sites and blocking the corrosion process. It is said [17] that the adsorption of organic compounds can be described by a process of physical adsorption and chemisorption. Physical adsorption requires the presence of both an electrically charged metallic surface and charged species into electrolyte, and the chemisorption involves charge sharing or charge transfer from the fatty-amide molecules to the metal surface to form a coordinate type of bond. The molecular structure of the unsaturated fatty-amides suggests that adsorption may occur through the unsaturation present on the carbon atoms of the oily tail. When the alkyl chain is saturated (stearic amide), the amide group resides on the metal surface with alkyl chain stretching out upwards into the electrolyte in a more perpendicular manner, if the alkyl chain is unsaturated (oleic and linoleic amide), the p-orbital of double bond can interact with the vacant d-orbital of metal, and the metal surface can be covered by amide group as the alkyl chains, and the continuous monolayer can efficiently prevent the diffusion of corrosive species, such as H_2O, H^+, Cl^-, and HCO_3^-. So the corrosion would be largely inhibited.

3.5. Corrosion Monitoring Real-Time. Figure 14 shows the variations of corrosion rate as determined by LPR measurements with time for carbon steel exposed to CO_2-saturated (3% NaCl + diesel) emulsion at 50°C, with the different fatty-amides. After 1.5 h of exposure, the fatty-amides were added and monitoring was carried out for 24 hours. With respect

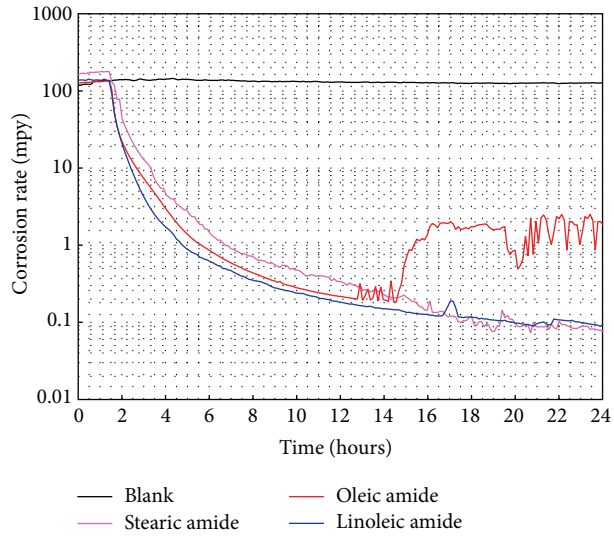

FIGURE 14: Variations of corrosion rate as determined by LPR measurements (*monitoring real-time*) with time for 1018 carbon steel exposed to CO_2-saturated (3% NaCl + diesel) emulsion at 50°C, with fatty-amides.

to blank, it is observed that its corrosion rate increases until 5.5 hours (from 120 mpy to 140 mpy) and then tends to slowly decrease to 125 mpy as time passes. Figure 14 shows that the corrosion rates fall rapidly two orders of magnitude after that the fatty-amides were added. The time required for this is, three hours for linoleic amide, four hours for oleic amide and, five hours for stearic amide. After that, the corrosion rates decrease slowly one order of magnitude more until the final of test for both stearic and linoleic amides. Similar corrosion rates were obtained with both amides after 16 hours. Until 13 hours of test, the effectiveness of inhibitors was based on the

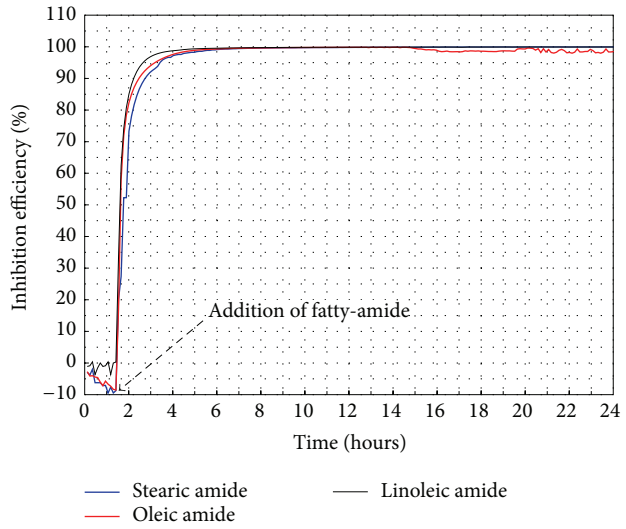

Figure 15: Variations of inhibition efficiency as determined by LPR measurements (*monitoring real-time*).

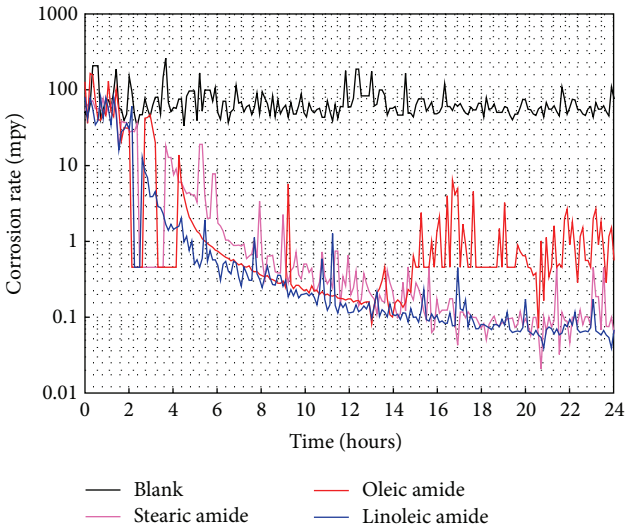

Figure 16: Variations of corrosion rate as determined by HDA measurements (*monitoring real-time*) with time for carbon steel exposed to CO_2-saturated (3% NaCl + diesel) emulsion at 50°C, with the different fatty-amides.

degree of unsaturation of the oil chain. However, after this point, oleic amide showed instability and the corrosion rate increased to 1-2 mpy.

Figure 15 shows the variation in the inhibition efficiency of the fatty-amides versus time (from LPR measurements of Figure 14). Its interpretation is in accordance with those discussed from the LPR measurements (Figure 14). However, it may be observed that although the oleic amide showed instabilities, the effectiveness of all fatty-amides is greater than 95% after two hours and about 99% during the rest of the corrosion test.

Figure 16 shows the variations of corrosion rate as determined by HDA measurements with time for carbon steel

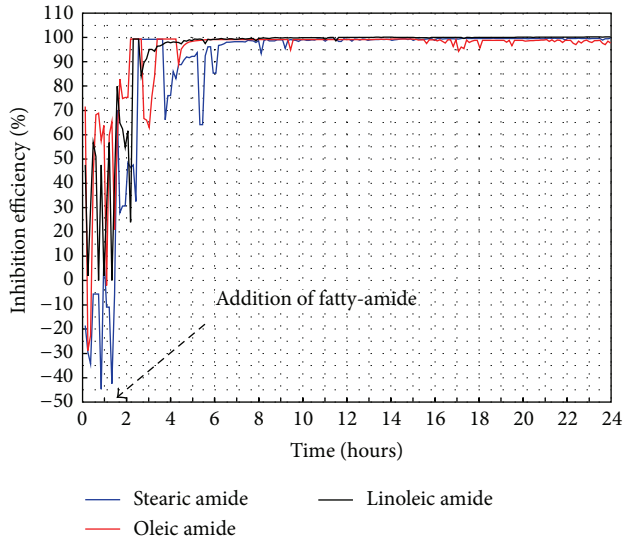

Figure 17: Variations of inhibition efficiency as determined by HDA measurements (*monitoring real-time*).

exposed to CO_2-saturated (3% NaCl + diesel) emulsion at 50°C, with the different fatty-amides. In general the corrosion rates obtained by the HDA technique followed a similar trend to those obtained by LPR. It is important to observe that in the case of the measurements with fatty-amides, regardless of the observed disturbances, the average corrosion rate values estimated from HDA are practically the same as those obtained values by LPR. In this case the calculations are made using the estimated values of anodic and cathodic Tafel slopes, obtained from the HDA technique. On the other hand, for the calculation of corrosion rate from LPR measurements, a value of 120 mV for both anodic and cathodic Tafel slopes was used. Disturbances observed can be interpreted as adsorption-desorption processes leaving active sites on the metal surface. These adsorption-desorption processes can affect the E_{corr} values and therefore the values of the Tafel slopes. Therefore it is more desirable to use instantaneous values Tafel slopes than using fixed values. The use of constant values will show a smoothed trend which do not allow observing the transient processes. In this sense, it is worth noting that, on average, the amplitude of the transients was lower with the linoleic amide, followed by the oleic amide, and finally by the stearic amide. This indicates that the unsaturation of the oil tail influences the effectiveness of the fatty-amides as inhibitor.

Similarly, in Figure 17 is shown the variation of the efficiency of the fatty-amides versus time, from measurements of HDA (Figure 16). Efficiency curves show many transients which can be interpreted as a measure of the adsorption stability of the fatty-amides onto the metallic surface. It can be seen that the time required for an apparent steady state was 1.5 hours for the linoleic amide, 3.0 hours for the oleic amide, and 4.5 hours for stearic amide. From this time, the effectiveness of the fatty-amides is greater than 95% and not the two hours as indicated by LPR measurements. That is, the stability of the adsorption process is a function of the unsaturation present in the oily tail of the fatty-amide. The adsorption-desorption

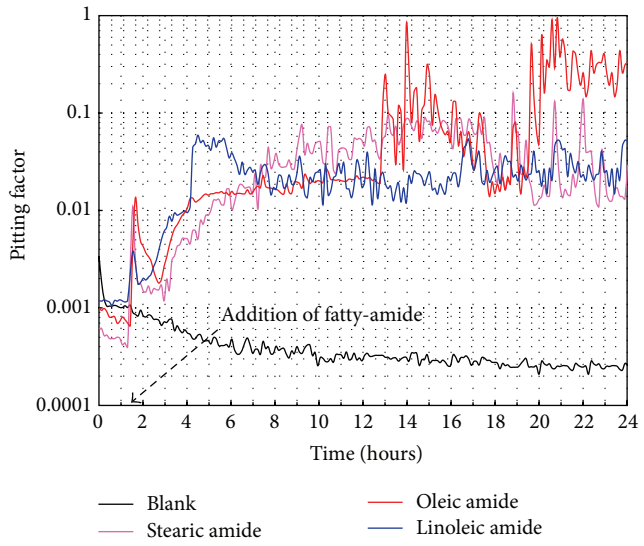

FIGURE 18: Variations of PF data with time for 1018 carbon steel exposed to CO_2-saturated (3% NaCl + diesel) emulsion at 50°C, with the different fatty-amides.

transients decrease as the number of unsaturation of the oily tail is higher. Again, it is more desirable to use instantaneous values Tafel slopes than using fixed values.

From comparison of the effectiveness curves (Figures 5, 15, and 17), it can be seen that the efficiency calculation from R_p measurements (without using Tafel slopes) is closer to those values obtained from HDA measurements. The differences are due to the sampling frequency used. For R_p measurements it was every 60 minutes, and for HDA measurements every 7 minutes. Therefore, in order to determine the efficiency of corrosion inhibitors, it is possible to suggest R_p measurements, rather corrosion rate measurements using fixed values Tafel constants.

Figure 18 shows the PF variations with time from EN and HDA data for carbon steel exposed to CO_2-saturated (3% NaCl + diesel) emulsion at 50°C, with the different fatty-amides. According to the plot, in the absence of fatty-amide, PF values for carbon steel are lower than 0.01 and show a tendency to decrease with time, where these PF values correspond to a general corrosion mechanism. However, during the first few minutes after the addition of fatty-amides, the PF values showed a sharp increment, reaching greater values than those obtained in solution without fatty-amides. After that, PF values decreased and subsequently increased to values between 0.01 and 0.1 for stearic amide and linoleic amide, where these values correspond to a mechanism of general corrosion with slight pitting attack. However, with oleic amide, the values ranged from 0.01 to 1.0, indicating pitting attack. Overall, the addition of all inhibitors produced an increase in PF values. These PF values suggested that a pitting-like process might be occurring at the electrode surface. It can be seen that the linoleic amide (two unsaturations) showed the most stable behavior; that is, its PF values tend to a constant value and the amplitude of the transients is lower.

4. Conclusions

Electrochemical impedance spectroscopy and real-time corrosion measurements were very useful tools to evaluate the effect of the double bonds into the hydrocarbon chain of the fatty-amides on the corrosion performance of carbon steel in CO_2-saturated (3% NaCl + 10% diesel) emulsion at 50°C. EIS results demonstrated that the unsaturation present in the oily tail contributes to the efficiency of fatty-amides because they can be adsorbed on the metal surface by a flat-adsorption process reducing the presence of active sites and blocking the corrosion process. When the alkyl chain is saturated the amide group resides on the metal surface with alkyl chain stretching out upwards into the electrolyte; if the alkyl chain is unsaturated the metal surface can be covered by amide group as the alkyl chains, and the continuous monolayer can efficiently prevent the diffusion of corrosive species. Real-time corrosion measurements indicated that the combination of LPR, HDA, and EN is suitable for the study of corrosion inhibitors in CO_2-saturated brine solutions in the presence of diesel. HDA technique is a promising method both for corrosion rate monitoring and to evaluate the efficiency of the inhibitors, showing fast response in real-time to small changes in the chemistry of the environment (with or without inhibitors).

Conflict of Interests

The authors declare that there is no conflict of interests regarding the publication of this paper.

Acknowledgment

Financial support from Consejo Nacional de Ciencia y Tecnología (CONACYT, México) (Project 198687) is gratefully acknowledged.

References

[1] M. Heydari and M. Javidi, "Corrosion inhibition and adsorption behaviour of an amido-imidazoline derivative on API 5L X52 steel in CO_2-saturated solution and synergistic effect of iodide ions," *Corrosion Science*, vol. 61, pp. 148–155, 2012.

[2] M. P. Desimone, G. Gordillo, and S. N. Simison, "The effect of temperature and concentration on the corrosion inhibition mechanism of an amphiphilic amido-amine in CO_2 saturated solution," *Corrosion Science*, vol. 53, no. 12, pp. 4033–4043, 2011.

[3] S.-H. Yoo, Y.-W. Kim, K. Chung, S.-Y. Baik, and J.-S. Kim, "Synthesis and corrosion inhibition behavior of imidazoline derivatives based on vegetable oil," *Corrosion Science*, vol. 59, pp. 42–54, 2012.

[4] H. M. Abd El-Lateef, V. M. Abbasov, L. I. Aliyeva, E. E. Qasimov, and I. T. Ismayilov, "Inhibition of carbon steel corrosion in CO_2-saturated brine using some newly surfactants based on palm oil: experimental and theoretical investigations," *Materials Chemistry and Physics*, vol. 142, no. 2-3, pp. 502–512, 2013.

[5] L. M. Rivera-Grau, M. Casales, I. Regla, D. M. Ortega-Toledo, J. G. Gonzalez-Rodriguez, and L. Martinez Gomez, "CO_2 Corrosion inhibition by imidazoline derivatives based on coconut

oil," *International Journal of Electrochemical Science*, vol. 7, no. 12, pp. 13044–13057, 2012.

[6] P. B. Raja and M. G. Sethuraman, "Natural products as corrosion inhibitor for metals in corrosive media—a review," *Materials Letters*, vol. 62, no. 1, pp. 113–116, 2008.

[7] V. Jovancicevic, "Inhibition of carbon dioxide corrosion of mild steel by imidazolines and their precursors," *Corrosion*, vol. 55, no. 5, pp. 449–455, 1999.

[8] R. N. Butler, J. D. Thornton, and P. Moynihan, "Reaction of fatty acids with amines. Part 3. thermal reactions of oleic and elaidic acids (*cis*- and *trans*-octadec-9-enoic acids) with some 1,2-diamines: ready reversibility of imidazoline formation," *Journal of Chemical Research, SYNOP*, vol. 3, pp. 84–85, 1981.

[9] S. O. Bondareva, V. V. Lisitskii, N. I. Yakovtseva, and Y. I. Murinov, "Hydrolysis of 1,2-disubstituted imidazolines in aqueous media," *Russian Chemical Bulletin*, vol. 53, no. 4, pp. 803–807, 2004.

[10] J. A. Martin and F. W. Valone, "The existence of imidazoline corrosion inhibitors," *Corrosion*, vol. 41, no. 5, pp. 281–287, 1985.

[11] S. Ramachandran, B.-L. Tsai, M. Blanco, H. Chen, Y. Tang, and W. A. Goddard, "Self-assembled monolayer mechanism for corrosion inhibition of iron by imidazolines," *Langmuir*, vol. 12, no. 26, pp. 6419–6428, 1996.

[12] E. E. Ebenso, U. J. Ekpe, B. I. Ita, O. E. Offiong, and U. J. Ibok, "Effect of molecular structure on the efficiency of amides and thiosemicarbazones used for corrosion inhibition of mild steel in hydrochloric acid," *Materials Chemistry and Physics*, vol. 60, no. 1, pp. 79–90, 1999.

[13] R. D. Kane and S. Campbell, "Real-time corrosion monitoring of steel influenced by microbial activity (SRB) in simulated seawater injection environments," in *Proceedings of the CORROSION*, Paper No. 04579, p. 15, NACE International, New Orleans, La, USA, March 2004.

[14] D. C. Eden, D. A. Eden, I. G. Winning, and D. Fell, "Online, real-time optimization of corrosion inhibitors in the field," in *Proceedings of the Corrosion*, Paper no. 06321, NACE International, San Diego, Calif, USA, March 2006.

[15] I. Gurappa, "Characterization of different materials for corrosion resistance under simulated body fluid conditions," *Materials Characterization*, vol. 49, no. 1, pp. 73–79, 2002.

[16] O. L. Riggs Jr., *Corrosion Inhibition*, C.C. Nathan, Houston, Tex, USA, 2nd edition, 1973.

[17] M. A. Amin, M. A. Ahmed, H. A. Arida et al., "Monitoring corrosion and corrosion control of iron in HCl by non-ionic surfactants of the TRITON-X series. Part III. Immersion time effects and theoretical studies," *Corrosion Science*, vol. 53, no. 5, pp. 1895–1909, 2011.

[18] M. S. Al-Otaibi, A. M. Al-Mayouf, M. Khan, A. A. Mousa, S. A. Al-Mazroa, and H. Z. Alkhathlan, "Corrosion inhibitory action of some plant extracts on the corrosion of mild steel in acidic media," *Arabian Journal of Chemistry*, vol. 7, no. 3, pp. 340–346, 2014.

[19] H. Ma, S. Chen, B. Yin, S. Zhao, and X. Liu, "Impedance spectroscopic study of corrosion inhibition of copper by surfactants in the acidic solutions," *Corrosion Science*, vol. 45, no. 5, pp. 867–882, 2003.

[20] P. Bommersbach, C. Alemany-Dumont, J. P. Millet, and B. Normand, "Formation and behaviour study of an environment-friendly corrosion inhibitor by electrochemical methods," *Electrochimica Acta*, vol. 51, no. 6, pp. 1076–1084, 2005.

[21] J. E. G. González and J. C. Mirza-Rosca, "Study of the corrosion behavior of titanium and some of its alloys for biomedical and dental implant applications," *Journal of Electroanalytical Chemistry*, vol. 471, no. 2, pp. 109–115, 1999.

[22] L. M. Rivera-Grau, M. Casales, I. Regla et al., "Effect of organic corrosion inhibitors on the corrosion performance of 1018 carbon steel in 3% NaCl solution," *International Journal of Electrochemical Science*, vol. 8, no. 2, pp. 2491–2503, 2013.

[23] J. Porcayo-Calderon, M. Casales-Diaz, L. M. Rivera-Grau, D. M. Ortega-Toledo, J. A. Ascencio-Gutierrez, and L. Martinez-Gomez, "Effect of the diesel, inhibitor and CO_2 additions on the corrosion performance of 1018 carbon steel in 3% NaCl solution," *Journal of Chemistry*, vol. 2014, Article ID 940579, 10 pages, 2014.

[24] D. M. Ortega-Sotelo, J. G. Gonzalez-Rodriguez, M. A. Neri-Flores, M. Casales, L. Martinez, and A. Martinez-Villafañe, "CO_2 corrosion inhibition of X-70 pipeline steel by carboxyamido imidazoline," *Journal of Solid State Electrochemistry*, vol. 15, no. 9, pp. 1997–2004, 2011.

[25] M. A. Amin, M. A. Ahmed, H. A. Arida, T. Arslan, M. Saracoglu, and F. Kandemirli, "Monitoring corrosion and corrosion control of iron in HCl by non-ionic surfactants of the TRITON-X series. Part II. Temperature effect, activation energies and thermodynamics of adsorption," *Corrosion Science*, vol. 53, no. 2, pp. 540–548, 2011.

[26] J. E. Ferrer and L. Victori, "Oxygen evolution reaction on the iridium electrode in basic medium studied by electrochemical impedance spectroscopy," *Electrochimica Acta*, vol. 39, no. 4, pp. 581–588, 1994.

[27] J. Zhang, J. Liu, W. Yu, Y. Yan, L. You, and L. Liu, "Molecular modeling of the inhibition mechanism of 1-(2-aminoethyl)-2-alkyl-imidazoline," *Corrosion Science*, vol. 52, no. 6, pp. 2059–2065, 2010.

[28] W. Villamizar, M. Casales, J. G. Gonzalez-Rodriguez, and L. Martinez, "CO_2 corrosion inhibition by hydroxyethyl, aminoethyl, and amidoethyl imidazolines in water-oil mixtures," *Journal of Solid State Electrochemistry*, vol. 11, no. 5, pp. 619–629, 2007.

[29] L. D. Paolinelli, T. Pérez, and S. N. Simison, "The effect of pre-corrosion and steel microstructure on inhibitor performance in CO_2 corrosion," *Corrosion Science*, vol. 50, no. 9, pp. 2456–2464, 2008.

[30] H. Ma, X. Cheng, G. Li et al., "The influence of hydrogen sulfide on corrosion of iron under different conditions," *Corrosion Science*, vol. 42, no. 10, pp. 1669–1683, 2000.

[31] W. Villamizar, M. Casales, J. G. Gonzales-Rodriguez, and L. Martinez, "An EIS study of the effect of the pedant group in imidazolines as corrosion inhibitors for carbon steel in CO_2 environments," *Materials and Corrosion*, vol. 57, no. 9, pp. 696–704, 2006.

[32] A. Y. Musa, R. T. T. Jalgham, and A. B. Mohamad, "Molecular dynamic and quantum chemical calculations for phthalazine derivatives as corrosion inhibitors of mild steel in 1 M HCl," *Corrosion Science*, vol. 56, pp. 176–183, 2012.